
Riemann Problem for the Euler Equation with Non-Convex Equation of State including Phase Transitions

Wolfgang Dahmen, Siegfried Müller, and Alexander Voß

Institut für Geometrie und Praktische Mathematik, RWTH Aachen,
Templergraben 55, D-52056 Aachen, Germany
dahmen,mueller,voss@igpm.rwth-aachen.de

Summary. An exact Riemann solver is developed for the investigation of non-classical wave phenomena in BZT fluids and fluids which undergo a phase transition. Here we outline the basic construction principles of this Riemann solver employing a general equation of state that takes negative nonlinearity and phase transition into account. This exact Riemann solver is a useful validation tool for numerical schemes, in particular, when applied to the aforementioned fluids. As an application, we present some numerical results where we consider flow fields exhibiting non-classical wave phenomena due to BZT fluids and phase transition.

1 Introduction

The dynamics of compressible flows has a strong influence on the design of aircraft and turbomachinery. In many applications the fluid is modeled by a perfect gas. In the range of perfect gas theory only two types of waves are possible and allowed by the entropy inequality, the *compression shock* and the *centered expansion fan* or *rarefaction wave*. A compression shock is a discontinuity where the pressure of the fluid increases while the shock is passing, whereas in a rarefaction wave the pressure decreases and the wave shape forms a fan.

However, the perfect gas model is no longer appropriate when dealing with so-called BZT fluids characterized by a large heat capacity, e.g., high molecular fluorocarbons and hydrocarbons. These fluids exhibit a region in the phase space where the isentropes in the pressure-volume plane are non-convex, see Figure 2. It is also referred to as region of *negative nonlinearity*. From experiments, see [BBKN83], it is known that there may occur non-classical effects such as *expansion shocks* and *compression fans*, as well as waves composed of adjacent shocks and rarefaction parts. In short, most of the classical inequalities and effects are reversed. In addition, below the critical point in the phase space, see Figure 2, liquid and vapor co-exist in a so-called

mixture region. One well known example is the heating of water, where at a certain temperature and pressure the water starts to vaporize and further heating does not result in hotter water but in more vapor. The temperature of the steam increases again, when all water has vaporized.

Due to the phase change at the phase boundary new phenomena such as liquefaction shocks, shock splitting, rarefaction shocks, complete evaporation shocks and liquid-evaporation waves have been observed, cf. [DTMS79, TK83, TCK86, TCM⁺87]. In this range we need an equation of state (EOS) which is able to model the negative nonlinearity of BZT fluids as well as phase transition.

In order to investigate these phenomena analytically, we consider the exact solution to a Riemann problem for compressible fluid flow where we employ a general EOS. 'Exact' means, the Riemann solution is based on wave curve analysis rather than on numerical approximations. Such an exact Riemann solver is helpful in many respects. First of all, it may serve as a validation tool for numerical schemes. Moreover, it can be used to determine initial conditions for experiments exhibiting effects such as, for instance, a liquefaction shock.

The general concept of constructing an exact Riemann solution is well-known, namely to construct the nonlinear wave curves corresponding to the nonlinear characteristic fields and to determine the intersection states in the pressure-velocity plane, cf. [MP89]. However, it has been an open problem so far *how* to construct the wave curves itself in this general setting including phase transition. If only negative nonlinearity is taken into account, their construction is well-known due to Wendroff [Wen72b] and Liu [Liu75]. In case of phase transition the wave curves are no longer smooth curves but they suffer kinks at the phase boundaries. These kinks cause jumps in the characteristic speeds which makes the construction of the waves much more difficult. Within the present project we extend for the first time the general concept of the wave composition and construction to this nonsmooth case. Here we confine to some basic principles motivated by a characteristic example. More details as well as analytical results concerning this subject can be found in [Voßa].

Realizing an exact Riemann solver for the Euler equations equipped with an EOS, including phase transition, requires a number of modules also needed for numerical schemes, such as an efficient evaluation of physical quantities, e.g., temperature and energy, for states inside the mixture region. For this purpose the C++-library `xrms` has been developed, see [Voßb]. This library has been incorporated into the QUADFLOW solver, cf. [BGMH⁺03].

The outline of the paper is as follows. First of all, we introduce retrograde and BZT fluids in Section 2 and summarize some characteristic features. In order to model these fluids we present a simplified real gas model in Section 3, based on the van der Waals EOS where we incorporate Maxwell's construction principle to resolve the unphysical region of ellipticity. Here the states in the mixture region are modeled in thermodynamical equilibrium. In Section 4 we outline the basic construction principles of the Riemann solver employing a

general EOS, taking negative nonlinearity and phase transition into account. Finally, we present some numerical results in Section 5 where we consider flow fields in BZT fluids exhibiting non-classical wave phenomena.

2 Retrograde and BZT Fluids

The material properties are characterized by the EOS. Certain constraints on the EOS are imposed by the principle of thermodynamics. Here, we confine ourselves to thermodynamical equilibrium, i.e., the internal specific energy $\mathbf{e} = \mathbf{e}(\mathbf{v}, \mathbf{s})$ of an equilibrium state is related to the specific entropy \mathbf{s} and the specific volume \mathbf{v} .

According to the *fundamental thermodynamic identity* the internal specific energy is characterized by

$$d\mathbf{e} = -p d\mathbf{v} + T d\mathbf{s}, \quad (1)$$

where the pressure p and the temperature T are defined by the partial derivatives of \mathbf{e}

$$p(\mathbf{v}, \mathbf{s}) := -\mathbf{e}_{\mathbf{v}}(\mathbf{v}, \mathbf{s}), \quad T(\mathbf{v}, \mathbf{s}) := \mathbf{e}_{\mathbf{s}}(\mathbf{v}, \mathbf{s}). \quad (2)$$

In contrast to regular fluids such as air, non-regular fluids exhibit anomalies in the T - \mathbf{s} diagram and in the p - \mathbf{v} diagram. These fluids are characterized by a large molar heat capacity, e.g., high-molecular hydrocarbons and fluorocarbons. In the literature, we distinguish between *retrograde fluids* and *BZT-fluids*.

2.1 Retrograde Fluids

Retrograde fluids are characterized by an overhang of the saturated-vapor curve in the T - \mathbf{s} -diagram. For a regular fluid the entropy increases with decreasing temperature along the saturated-vapor curve. In contrast to this, retrograde fluids exhibit some part of the saturated-vapor curve where the entropy decreases with decreasing temperature, see Figure 1. This implies that for regular fluids condensation takes place on *isentropic expansion* whereas for retrograde fluids it takes place on *isentropic compression*, at least in these particular regions.

By means of the characteristic heat capacity

$$\tilde{c}_{\mathbf{v}} = \frac{c_{\mathbf{v}}^0(T_c)}{\mathcal{R}}$$

retrograde fluids can be distinguished from regular fluids. Here $\tilde{c}_{\mathbf{v}}$ is defined by the ideal-gas heat capacity at the thermodynamic critical temperature T_c normalized by the gas constant \mathcal{R} . It was found by Lambrakis [Lam72] that fluids exhibit the overhang whenever the characteristic heat capacity exceeds $\tilde{c}_{\mathbf{v}} \geq 11.2$.

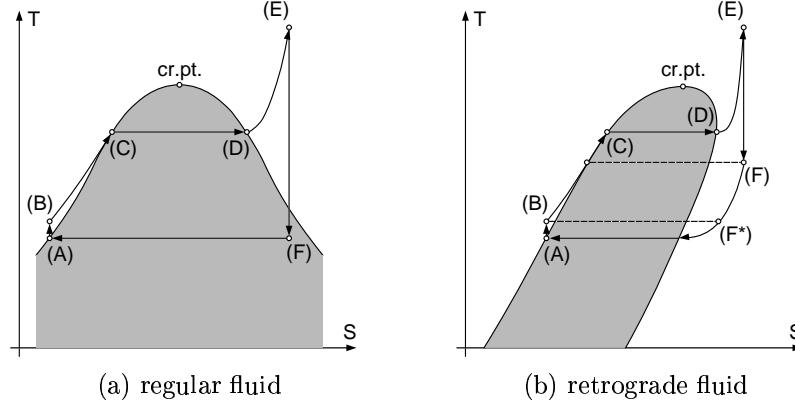
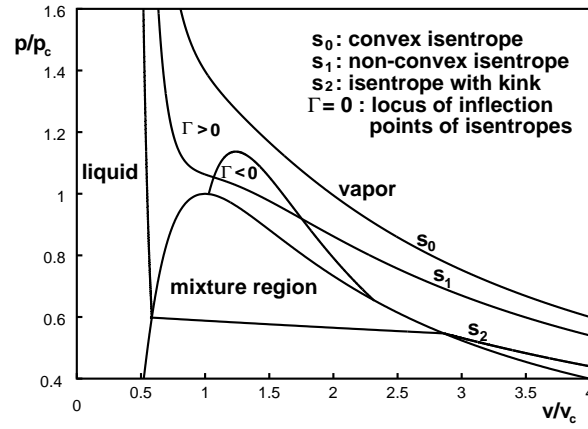


FIGURE 1. Clausius-Rankine-cycles.

2.2 BZT Fluids

BZT fluids are a subgroup of retrograde fluids. They are named after Bethe (1942), Zel'dovich (1946), Thompson (1971). For BZT fluids the curvature of the saturation curve is so intense that it leads to a concave bending of the isentropes near the critical point in the p - v -diagram, see Figure 2, i.e., the isentropes are locally non-convex.

Fig. 2. Isentropes of a BZT Fluid in p - v diagram

This is in contrast to the behavior of the most common fluids where isentropes are convex. A measure for the bending is the *fundamental derivative of gas dynamics*

$$\Gamma := \frac{v^3}{2c^2} p_{vv}(v, s) = \frac{v}{2} \frac{p_{vv}(v, s)}{-p_v(v, s)} \quad (3)$$

which becomes negative in a region near the critical point. Here, c denotes the speed of sound defined by

$$c^2 := -v^2 p_v(v, s). \quad (4)$$

Note, that the so-called region of *negative nonlinearity*, i.e., $\Gamma < 0$, is located in the vapor phase at the curve of saturated vapor, see Figure 2.

Another feature of BZT fluids is that isentropes inside the mixture region may cross the curve of saturated vapor such that the isentropes suffer a non-convex kink. This is different for other fluids whose isentrope will never cross the saturated vapor curve. For more details on BZT fluids see, for instance, Thompson [Tho91].

3 Physical Model

For our investigations the fluid is modeled by the van der Waals EOS. This gives a qualitatively good representation of the fluid in various important regions, namely the regimes of high compression, the area with negative nonlinearity near the critical point regarding BZT fluids and the mixture region to allow for phase transition.

3.1 Van der Waals Equation of State

A vital assumption of the ideal gas model is that the particles are non-interacting mass points, i.e., an appreciable force acts on them only during a collision. Furthermore, the volume of the particles is negligible compared to the total volume occupied by the gas. This is no longer valid if the density is so high that the distance between two particles is of the order of their interaction diameter. Such extreme densities can be reached during the collapse of a bubble. In this case, the range of validity of the ideal gas model is exceeded.

The van der Waals EOS is an extension of the ideal gas model with two material parameters a and b to take into account the attraction of particles and the reduction of free volume. The thermal EOS is determined by

$$p(v, T) = \frac{\mathcal{R} T}{v - b} - \frac{a}{v^2} \quad (5)$$

with pressure p , temperature T , specific volume v , specific gas constant \mathcal{R} , internal pressure a/v^2 and covolume b . The internal pressure is subtracted from the pressure to take into account that the attraction of particles diminishes the pressure. The covolume b reduces the volume v to the available free volume $v - b$. The caloric EOS reads

$$e(v, T) = e_0 + \int_{T_0}^T c_v(T) dT - \frac{a}{v} \quad (6)$$

where c_v denotes the heat capacity at constant volume and e the internal energy. Together with the fundamental identity of gas dynamics (1) we conclude

$$s(v, T) = e_0 + \int_{T_0}^T \frac{1}{T} c_v(T) dT$$

with e_0 the heat of formation.

3.2 Mixture Region

Since we want to apply the van der Waals EOS to gases and liquids as well, there is a need for describing what happens in the region of phase transition. In Figure 3 three isotherms are plotted in the p - v diagram, corresponding to (i) a temperature above the critical temperature T_c , (ii) the critical temperature (the critical isotherm) and (iii) a temperature below T_c .

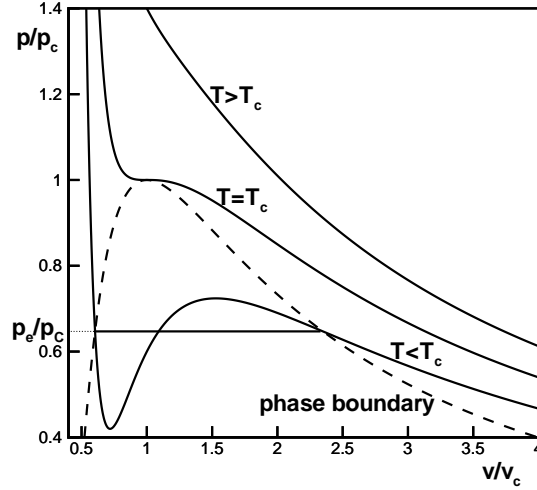


Fig. 3. Isotherms of a BZT-Fluid in p - v diagram

In the mixture region, liquid and gas are present in a continuously changing fraction where the fraction of liquid increases when the volume decreases. However, the original van der Waals equation shows an unphysical inclination in this area. This can be seen if we consider an isotherm for a temperature below the critical one. We observe two local extrema, called *spinodal points*. They correspond to the endpoints of supersaturated vapor (maximum) and overexpanded liquid (minimum), respectively. Between these two points

the derivative $p_v(v, T)$ is positive and, hence, physically excluded. In order to provide physically meaningful data, we calculate the equilibrium pressure $\bar{p} = \bar{p}(T)$, see Figure 3, as a function of the temperature using the *Maxwell's construction principle*:

$$\int_{\bar{v}_1}^{\bar{v}_2} p(v, T) dv = \bar{p} (\bar{v}_2 - \bar{v}_1), \quad p(\bar{v}_1, T) = p(\bar{v}_2, T) = \bar{p}.$$

By means of this system we determine for any $T \leq T_c$ the equilibrium pressure \bar{p} and the corresponding specific volumes \bar{v}_1 and \bar{v}_2 characterizing the phase boundary corresponding to saturated vapor and saturated liquid, respectively. In order to determine internal energy and entropy inside the mixture region we assume equilibrium. Hence, the corresponding states can be calculated by the convex combination of the equilibrium states at the phase boundary, see [Voßa], [Voßb] for details on the implementation. Note, that by this ansatz, we exclude the possibility of so-called metastable states.

4 The Riemann Problem of Gas Dynamics

In order to investigate analytically nonclassical wave phenomena such as expansion shocks and compression waves as well as wave splitting, we consider the Riemann problem for gas dynamics. In Lagrangian coordinates this problem can be formulated as

$$q_t + f(q)_x = 0$$

with piecewise constant initial data

$$q(0, x) = \begin{cases} q_l : x < 0 \\ q_r : x > 0 \end{cases}.$$

Here the vector of conserved quantities q and the flux $f(q)$ are determined by

$$q = (v, u, E)^T, \quad f(q) = (-u, p, pu)^T,$$

with the specific volume v , the velocity u , pressure p , the total energy $E = e + 0.5 u^2$ and the internal energy e . This system is closed by a general EOS

$$p = p(v, s), \quad p_v(v, s) < 0. \quad (7)$$

Here we assume that the isentrope is a strictly monotone function in order to ensure strict hyperbolicity of the underlying system of equations. According to standard assumptions of equilibrium thermodynamics we may express equivalently the pressure also in terms of specific volume and internal energy.

By now, the Riemann problem is well understood for the Euler equations that model equilibrium hydrodynamics. For an overview we refer to the review article by Menikoff and Plohr [MP89]. The general construction principle

for the Riemann solution is essentially based on the scale-invariance of the solution and the hyperbolicity of the governing equations of fluid motion. These properties require the solution to be composed of different waves in the time-space continuum which correspond to different characteristic velocities. Moreover, there exists a one-to-one correspondence between a single wave in the t - x diagram and the states in the phase space which can be connected by this wave. All of these states are lying on one-parametric curves and the solution of the Riemann problem is determined by the intersection points of the different curves each corresponding to a characteristic field in the phase space connecting the two initial states. Hence, the most crucial point in solving the Riemann problem analytically is the construction of the curves in phase space. To distinguish the respective settings in the course of the discussion we will consistently refer to one-parameter families of states in phase space as *curves* while speaking of *waves* in the x - t plane.

4.1 Characterization of Wave Curves

In order to characterize the different curve types we first introduce the characteristic speeds $\lambda_k(\mathbf{q})$, $k = 1, 2, 3$, as the k th eigenvalue of the Jacobian of $\mathbf{f}(\mathbf{q})$ which turn out to be

$$\lambda_1 = -\sqrt{-\mathbf{p}_v(v, \mathbf{s})} = -c/v < \lambda_2 = 0 < \lambda_3 = +\sqrt{-\mathbf{p}_v(v, \mathbf{s})} = c/v$$

where c denotes the sound speed defined in (4). The corresponding right eigenvectors are given by

$$\begin{aligned} \mathbf{r}_k &= \frac{1}{\lambda_k} (-1, \lambda_k, \mathbf{p} + \lambda_k \mathbf{u})^T, \quad k = 1, 3 \\ \mathbf{r}_2 &= (-\mathbf{p}_e(v, \mathbf{e}), 0, \mathbf{p}_v(v, \mathbf{e}))^T. \end{aligned}$$

Then the corresponding characteristic k -field is characterized by the variation of the characteristic velocity λ_k in the direction of the corresponding k th right eigenvector of the Jacobian of $\mathbf{f}(\mathbf{q})$, i.e.,

$$\alpha_k := \nabla \lambda_k \mathbf{r}_k, \quad k = 1, 2, 3.$$

These are determined by

$$\alpha_1 = \alpha_3 = \Gamma/v, \quad \alpha_2 = 0$$

where Γ denotes the fundamental derivative of gas dynamics defined in (3). Obviously, for a convex EOS, i.e., $\Gamma > 0$, we distinguish between two cases, namely, the k -field is *linearly degenerated*, i.e., $\alpha_k(\mathbf{q}) = 0$ for all \mathbf{q} , or the k -field is *genuinely nonlinear*, i.e., $\alpha_k(\mathbf{q}) \neq 0$ for all \mathbf{q} . In case of a non-convex EOS the nonlinear fields may locally degenerate, i.e., there are states $\bar{\mathbf{q}}$ in phase space such that $\alpha_k(\bar{\mathbf{q}}) = 0$.

4.2 Construction of an Exact Riemann Solution.

Next we give an idea on how to construct a Riemann solution for the Euler equations if non-genuine nonlinear fields and phase transition come into play. To focus on the main principles we restrict our characterization to some special cases, clarified by means of a comprehensive example. A complete description containing all cases for the Euler equations augmented with an EOS of van der Waals-type can be found in [Voßa]. In particular, we skip a discussion on uniqueness and existence and assume, that there is always a unique entropy solution.

4.3 Wave Curves

In general, the entropy solution of a Riemann problem for a hyperbolic system of m conservation laws can be constructed by considering the so-called *wave curves* $W_k : \mathbb{R} \rightarrow \mathbb{R}^m$, $k = 1, \dots, m$. These are parameterized curves connecting some initial state $q_k = W_k(0)$ with *all* “reachable” states.

Then the solution for a Riemann problem with initial data q_l and q_r is found, if there is a vector of parameters ξ_k , $k = 1, \dots, m$, connecting q_l and q_r , here from left to right, by means of the m wave curves, i.e.,

$$W_m(\dots W_2(W_1(q_l, \xi_1), \xi_2), \dots, \xi_m) = q_r.$$

In other words, each wave curve except the first one, starts at some intermediate state of the previous one and the crucial point is to find these states q_k , respectively the parameters ξ_k , cf. Figure 4.

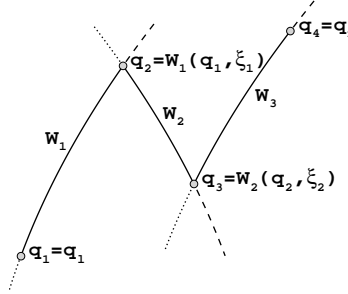


Fig. 4. Construction of the Riemann solution by means of wave curves.

In case of the Euler equations the problem can be reduced to the 1- and the 3-curve, because the 2-wave is always a contact discontinuity, where the pressure p and velocity u are constant. Therefore, the construction principle

in this case simplifies as follows: Compute the 1-wave, i.e., collect all states which *can be reached from* q_l . Simultaneously compute the 3-wave *backwards*, i.e., collect all possible intermediate states *from where one can reach* the end state q_r . The intersection point of the two waves projected onto the p - u plane is the origin of W_3 . Thus the parameters ξ_1 and ξ_3 and the solution respectively, are known.¹

4.4 Computation of Wave curves

At this point it remains to *compute* the wave curves. Using a *convex* EOS like the ideal gas law leads to wave curves composed of exactly one rarefaction and one shock branch. Here either side of the wave curve is referred to as a wave branch.

By changing the EOS to a non-convex one, for instance, to the van der Waals EOS, applied to BZT fluids, regions in phase space arise where the sign of the fundamental derivative becomes negative and the nonlinear k -fields degenerate. Regarding the wave branches this may cause the break-down of the classical curve types *rarefaction* and *shock* and implies various facts: firstly, a wave branch can be composed of so-called *wave parts*, that is a section of the wave branch with one wave type. Then the parameter range of the branch $[0, \xi_k]$ is partitioned into smaller parts $[\xi_k^j, \xi_k^{j+1}]$. The situation is shown in Figure 5. Secondly, the classical wave types are not sufficient to continue the

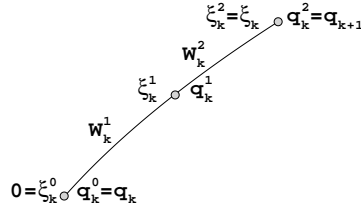


Fig. 5. Wave curve partitions of W_k .

wave curves in an admissible way. Therefore, a new part type *composite* has to be introduced, taking sonic shocks and rarefactions (see below) into account. The concept of composite waves was introduced first by Wendroff [Wen72a], [Wen72b] and Liu [Liu75]. Thirdly, in case of composites away from the phase boundaries, the wave curves are no longer twice but only once differentiable and at phase boundaries only continuous.

¹ For the sake of completeness, the parameter ξ_2 can be reconstructed from the known intermediate states.

4.5 Wave parts

A wave curve, or, more precisely, a wave branch may be composed of several wave parts. Each part is of either the type rarefaction R, shock H or composite C. They are defined, in short, as follows.

Rarefaction Curves

For the nonlinear fields, here $k = 1, 3$, we define the parameterized curve R_k as the solution to the ODE

$$\frac{\partial R_k}{\partial \xi}(\bar{q}, \xi) = r_k(R_k(\xi)), \quad R_k(\bar{q}, 0) = \bar{q},$$

i.e., as integral curve along the right eigenvector through a state \bar{q} . If λ_k is *not decreasing* along these curve, i.e., $d\lambda_k/d\xi \geq 0$, it is equivalent to the classical *rarefaction curve*. Such a curve is called *admissible* and it collects all states which can be connected to \bar{q} by a centered rarefaction fan.

Note, that when λ_k decreases along a wave part being part of a Riemann solution, thus would lead to (prohibited) folding of the solution in the x - t plane. Similarly, the usual parameterization $\xi = x/t$ is not appropriate when $d\lambda_k/d\xi$ vanishes along R_k .²

In case of the Euler equations a rarefaction curve parameterized by the pressure is obtained by solving

$$dq = \frac{1}{\lambda_k} r_k dp,$$

from a given state \bar{q} .

Using the fundamental identity of gas dynamics (1), we conclude that the entropy is constant along R_k , as long as it is admissible. Hence, a projection of R_k onto the p - v plane depicts the isentropes.

It can be shown, that the admissible branch of the rarefaction curve R_1 corresponds to the expansion branch ($dv > 0$, $dp < 0$) in case of positive nonlinearity ($\Gamma > 0$) and the compression branch ($dv < 0$, $dp > 0$) in case of negative nonlinearity ($\Gamma < 0$). The roles of positive and negative nonlinearity are reversed for the 3-field. Moreover, pressure and velocity are monotone functions inside the compression (expansion) branch of the rarefaction curve.

We emphasize that the above conclusions hold true as long as the rarefaction curve stays smooth. However, if the isentrope crosses the phase boundary, see Figure 2, then the rarefaction curve suffers a convex kink at the saturated-liquid curve and, in addition, in the case of BZT fluids a non-convex kink at the saturated-vapor curve. Hence, the sound speed and the characteristic speed, respectively, jump at the phase boundary.

² As a technical remark: it is important for the construction principle to know the sign of the characteristic fields *behind* such a state with $d\lambda_k/d\xi = 0$. Hence the parameterization must not depend on $\xi = x/t$.

Shock Curves

The set of discontinuities satisfying the *Rankine-Hugoniot conditions* is given by the *Hugoniot locus*

$$\mathcal{H}_k(\bar{\mathbf{q}}) := \{\mathbf{q} : \exists \sigma \in \mathbb{R} \quad \text{s.t.} \quad \mathbf{f}(\mathbf{q}) - \mathbf{f}(\bar{\mathbf{q}}) = \sigma(\mathbf{q} - \bar{\mathbf{q}})\},$$

where $\sigma = \sigma(\mathbf{q}, \bar{\mathbf{q}})$ denotes the *shock speed*.

For the Euler equations in Lagrangian coordinates the Rankine–Hugoniot conditions for the nonlinear k -fields read

$$\sigma^2 = -\frac{\Delta \mathbf{p}}{\Delta \mathbf{v}}, \quad \Delta \mathbf{e} + \left(\frac{\Delta \mathbf{p}}{2} + \bar{\mathbf{p}}\right) \Delta \mathbf{v} = 0. \quad (8)$$

Here, we use the notation $\Delta A = A - \bar{A}$ for an arbitrary quantity A . In particular, $\sigma \neq 0$ or, equivalently, $\Delta u \neq 0$, $\Delta p \neq 0$.

In order to determine the admissible branch of the Hugoniot curves, we consider the entropy jump. For a weak shock the entropy jump $\Delta \mathbf{s}$ is proportional to the third power of the pressure jump $\Delta \mathbf{p}$, i.e.,

$$\Delta \mathbf{s} = \frac{c^2}{6 v^3} \bar{\Gamma} \bar{\Gamma} (\Delta \mathbf{p})^3 + \mathcal{O}((\Delta \mathbf{p})^4),$$

see [Tho72]. According to the second law of thermodynamics, the entropy jump has to be positive, i.e., $\Delta \mathbf{s} > 0$, when the shock passes.

Hence, the pressure jump has to be positive ($\bar{\Gamma} > 0$) and negative ($\bar{\Gamma} < 0$), respectively, to fulfill the entropy condition. From this we conclude that for $\bar{\Gamma} > 0$ a *compression shock* ($\Delta \mathbf{p} > 0$, $\Delta \mathbf{v} < 0$) is admissible and for $\bar{\Gamma} < 0$ an *expansion shock* ($\Delta \mathbf{p} < 0$, $\Delta \mathbf{v} > 0$).

In order to analyze the uniqueness of the Riemann problem Smith [Smi79] introduced several conditions on the EOS referred to as *strong*, *medium* and *weak condition*, respectively. Menikoff and Plohr [MP89] verified that they are also important for discussing monotonicity of thermodynamic and hydrodynamic quantities along the Hugoniot locus. In particular, they proved that the following holds at a point on the compression branch of the Hugoniot locus, in the direction of increasing shock strength: (i) \mathbf{v} decreases monotonically if the strong condition holds; (ii) \mathbf{e} and \mathbf{u} increase monotonically if the medium condition holds and (iii) \mathbf{p} increases monotonically if the weak condition holds. So far, all materials known satisfy the weak condition. Therefore it makes sense to parameterize the wave curves by the pressure.

Moreover, it can be proven that the entropy \mathbf{s} is an extremum, if and only if the shock speed σ is an extremum. This does hold true at a point on a shock curve where it is smooth, see [MP89], Theorem 4.2. A variant is true even at points where the Hugoniot locus intersects the phase boundary. In the latter case the entropy \mathbf{s} increases with shock strength if and only if the shock speed σ increases with shock strength, provided that the weak condition holds at a point on the compression branch of a shock curve, see [MP89], Theorem 4.5.

Hence, the entropy as well as the shock speed vary monotonically along the admissible branch as is predicted by Liu's extended admissibility relations in [Liu76]. It is extremal, if and only if the shock becomes sonic. This coincides with the state where the second law of thermodynamics is violated marking the end of the admissible branch. Hence, we can use the variation of the shock speed as admissibility criterion of the shock.

Composite Curves

As we discussed above the nonlinear fields may degenerate at states where the fundamental derivative of gas dynamics vanishes, i.e., $\Gamma = 0$. Beyond this state the rarefaction curve is no longer admissible. In order to continue the wave curve, Wendroff [Wen72b] introduced the notion of a *composite curve*. Later on, Liu extended this concept to general hyperbolic conservation laws, see [Liu75]. Following Liu's definition, the composite locus is determined by

$$C_k(R_k, \bar{q}) = \{ q : \exists q^* \in R, q \in H(q^*) \text{ and } q \text{ is the first state on } H(q^*) \text{ with } \lambda_k(q^*) = \sigma(q^*, q) \}.$$

Since the shock is as fast as the characteristic speed of state q^* , each state q on C_k represents a wave in the x - t plane combined of a rarefaction up to q^* and an adjacent shock from q^* to q , see Figure 6. This locus is a one parameter

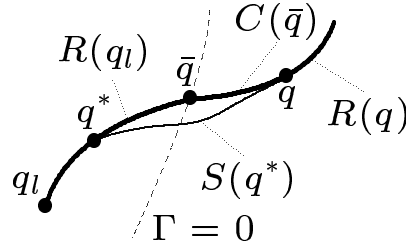


Fig. 6. Composite curve

family of states. In case that \bar{q} corresponds to a state where Γ vanishes, it can be proven that the composite curve is tangentially attached to the rarefaction curve R_k at \bar{q} , see [MV01]. The corresponding curve is admissible as long as (i) $\sigma(q^*, q) \neq \lambda_k(q)$ and (ii) q^* is not the origin of R_k , cf. [Liu75].

4.6 Admissible conditions

Knowing the construction principle, as well as the mathematical conditions on the wave parts, we want to collect the conditions for changing the wave types during the computation of the wave branch, or, raise the question, how

long is a wave part admissible? We shall see, that due to phase transition additional conditions arise.

No Phase transition. As mentioned before, a necessary condition for a rarefaction part to be admissible is that the wave speed λ_k increases along the wave part. Otherwise the solution would fold in the x - t plane. Increasing λ_k is tantamount to a fixed sign of the fundamental derivative Γ and if the rarefaction part never crosses a region where Γ changes its sign, the wave type does not change. At a state with vanishing derivative of λ_k , i.e., $\Gamma = 0$, the rarefaction part ends and a new composite part begins.

A similar speed condition has to hold along the shock part, namely, the shock speed σ_k has to decrease along the Hugoniot curve, which is the *extended Liu-condition*. It reduces to the well-known Lax criteria in case of a convex EOS. As mentioned before, if σ_k does not decrease anymore, the wave curve must have entered a region of negative nonlinearity before. Then the shock part ends here and the wave branch can be smoothly continued by a rarefaction part. The shock is called *sonic* because it travels with the same speed as the first state on the following rarefaction.

The new type composite is a set of shock states. In the current context such a wave part starts at a state \bar{q} where $\Gamma = 0$, and the wave part before must be a rarefaction part. Like a shock part, the composite part is admissible as long as the shock speed along the composite part is decreasing. If this is violated the next wave part is a rarefaction part again and the situation is similar to a sonic shock. It is known that the associated states at the preceding rarefaction part R are moving towards the origin of the rarefaction part. This leads to the other terminating condition for the composite part, i.e., the associated rarefaction state *is* the origin of R . Then the wave curve can be continued with a shock part where the shock origin is the origin of R .

Including Phase transition. So far we described the *non-convex* situation where the wave curves are smooth. It becomes even more complicated if the wave curves crosses a phase boundary. The good news is that, like in the smooth non-convex case, three types of wave parts suffice to construct a Riemann solution. The bad one is that the discontinuity of the characteristic speed λ_k as well as the possible change of the sign of nonlinearity across a phase boundary causes additional terminating conditions for wave parts. This is directly related to the question how to continue the wave branch. These topics are treated in mathematical detail in [Voßb]. Here we can only give a summary of the results by means of a table containing the different cases and terminating conditions, see Table 1.

As we mentioned above the monotonicity of the wave speed, denoted by s' , i.e., λ'_k or σ'_k , along the curve, is one of the main criteria to continue or terminate a wave part. One can find it in the first part of Table 1, the *admissible criteria*. They are in effect while a wave part is computed.

In some cases the wave speed s or its derivative s' jumps while crossing the phase boundary and it makes sense to speak of a quantity *before* $(\cdot)^-$ and *behind* $(\cdot)^+$ the boundary, depending on the parameterization. In the end

there is a final terminating condition. It emerges if a wave takes over another wave. This happens, for instance, if a shock wave crosses a phase boundary, the jump in shock speed is positive *and* behind the boundary the wave curve continues with a second shock part, see case H^[-]. Since the jump is positive and the shock speed is decreasing along the second part, it may happen, that the speed coincides with the last shock speed of the first shock part. In this case the solution cannot consist of two shocks anymore but the first shock part will be continued and it takes over the second one. Otherwise it would result in a folding of the second shock in the $x-t$ plane.

This means, there are terminating conditions depending on the history of the wave curve, respectively on wave speeds passed on previous wave parts. To handle these speeds appropriately the idea of a *stack* is helpful. Such a stack works like a book pile. One can put some book on top of it (push) or remove some from the top (pop). Now some conditions, namely, the one where the wave speed jumps, *push speed* on the stack while all overtaking cases *pop speed*. Consequently, the current shock and composite speeds have to be compared to the speeds on the stack, and this is denoted by $s \neq s_{[\text{old}]}$ in the first part of the table and by $s = s_{[\text{old}]}$ in the second part.

types of wave parts and conditions in effect		
R	$s' > 0$, curve is smooth	
H	$s' < 0$, $s \neq s_{[\text{old}]}$	
C	$s' < 0$, $s \neq s_{[\text{old}]}$, origin of corresponding R is not reached	
abbreviations for terminating conditions		succ. remark
R ^[m]	monotonicity (m) of s broken, i.e., $s' = 0$	C
R ^[++]	phase boundary crossed, $s'^+ > 0$, $s^+ > s^-$	R push s^-
R ^[+-]	phase boundary crossed, $s'^+ > 0$, $s^+ < s^-$	C
R ^[-+]	phase boundary crossed, $s'^+ < 0$, $s^+ > s^-$	H push s^-
R ^[--]	phase boundary crossed, $s'^+ < 0$, $s^+ < s^-$	C
R ^[e]	external (e) condition fulfilled, i.e., a given state is reached or a maximum number of states is computed.	
H ^[m]	monotonicity (m) broken, i.e., $s' = 0$	R push s^-
H ^[+]	phase boundary crossed, $s'^+ > 0$	R push s^-
H ^[-]	phase boundary crossed, $s'^+ < 0$	H push s^-
H ^[R]	overtaken by R, i.e., $s = s_{[\text{old}]}$	C pop
H ^[H]	overtaken by H, i.e., $s = s_{[\text{old}]}$	H pop
H ^[C]	overtaken by C, i.e., $s = s_{[\text{old}]}$	C pop
H ^[e]	external (e) condition fulfilled	
C ^[m]	monotonicity (m) broken, i.e., $s' = 0$	R push s^-
C ^[+]	phase boundary crossed, $s'^+ > 0$	R push s^-
C ^[-]	phase boundary crossed, $s'^+ < 0$	H push s^-

$C^{[H]}$	overtaken by H, i.e., $s = s^{[old]}$	H	pop
$C^{[C]}$	overtaken by C, i.e., $s = s^{[old]}$	C	pop
$C^{[b]}$	begin (b) of corresponding R reached	H	
$C^{[e]}$	external (e) condition fulfilled		

Table 1: Terminating conditions for wave parts.

4.7 Example

We would like to give an example to demonstrate the interaction between different wave parts along one wave curve. Since in case of the Euler equations both nontrivial waves are treated similarly, we can confine the discussion to only one family, here $k = 1$. The EOS used is the van der Waals one and the fluid is the BZT fluid PP10. The wave curves are parameterized by the pressure.

Figure 7(a) shows the wave curve projected into the phase diagram, i.e., the p - v plane. Here we can see which physical regions are crossed and which types of phases and nonlinearities are present at every state and part of the curve. Figure 7(b) specifies the wave speed along the curve. This clarifies the terminating condition for a wave part and in which way the wave curve is continued. Figure 8 reflects the evolution of the solution structure (here: pressure) along the wave curve in space at a constant time. Note, that the solution can consist only of one shock, even if the wave curve is composed of various wave parts of different type. To this end we fix one part of initial Riemann data, q_l , and vary the right state $q_r = q_r^i$. In each case, we calculate the exact solution, and compare it with a numerical one, obtained by the WAF method.

The wave curve starts at ξ_k^0 near the critical point in the liquid phase and is calculated with decreasing pressure as the curve parameter, cf. Figure 7(a). The first part is the rarefaction part R_1 . Here the wave speed increases along the curve, cf. Figure 7(b), up to the point ξ_k^1 . It terminates, because the wave curve crosses the saturated-liquid phase boundary, that can be seen at best in the small zoomed window in Figure 7(a). Hence, the solution in the x - t plane, corresponding to the right state $q_r = q_1$ taken from R_1 , is a rarefaction wave, cf. Figure 8(a). The wave is very fast and looks like a shock because the isentropes are very steep in this region, but it is still smooth.

At the phase boundary the corresponding eigenvalue is discontinuous. Thus the speed jumps, cf. Figure 7(b), but to a higher value, implying that the wave curve is continued with a second rarefaction wave, R_2 . Figure 8(b), calculated for $q_r = q_2$, shows, that the discontinuity in the wave speed leads to a splitting of the two rarefaction parts. Inside the mixture region the isentrope remains convex and the rarefaction part R_2 lasts up to the saturated-vapor boundary,

that is at ξ_k^2 .

Now the wave speed is decreasing and the next wave part is the composite part C_2 corresponding to the rarefaction part R_2 from inside the mixture. We expect a Riemann solution for data $q_r = q_3$ to split into two waves and the right one to be composed of a rarefaction and an adjacent shock, like in Figure 8(c). The composite part ends at the state ξ_k^3 , because we reach the beginning of the rarefaction part R_2 with the corresponding rarefaction states. It can be seen from the wave speed diagram that this is exactly the case when the speed at ξ_k^3 is equal to the speed of the first state on R_2 .

In a certain sense the gap in the speed is by-passed with a shock part H_1 from ξ_k^3 to ξ_k^4 . This is in agreement with the observation that along the last composite part C_2 the exact solutions of the type as shown in Figure 8(c) are combined of a shock with increasing strength and a vanishing rarefaction part. Here the shock part continues this evolution. In the $x-t$ plane, the solution to $q_r = q_4$ is still split into two waves, but the splitting itself decays, i.e., the wave speeds are approaching, cf. Figure 8(d). In the end the speed of the shock part reaches the speed of the first rarefaction part R_1 at ξ_k^4 , cf. Figure 7(b).

Now, if not terminated, the shock would be faster than the last rarefaction states, and this means a folding in the $x-t$ plane. Hence we continue the wave curve with a composite part again, C_1 , now corresponding to the first rarefaction part R_1 . Such a solution is given for the Riemann data $q_r = q_5$ in Figure 8(e).

Like before, the corresponding rarefaction R_1 is eaten up by the composite states and we continue the wave curve from the point, where the speed of the first state of the rarefaction is reached, here at ξ_k^5 , with a new shock part H_2 . The speed is decreasing and a solution to one of these shock states $q_r = q_6$ is provided by Figure 8(f).

Since the wave curve crossed the region of negative nonlinearity before, the shock may become sonic. This happens at ξ_k^6 . The following rarefaction part R_3 is adjacent to the last shock state and because there are no further anomalies in phase space the wave curve remains a rarefaction part for all parameter greater than ξ_k^6 . Hence, the last possible wave curve type is shown in Figure 8(g).

parameter range	wave part	terminating condition	figure
$[\xi_k^0, \xi_k^1]$	R_1	$R^{[++]}$	8(a)
$[\xi_k^1, \xi_k^2]$	R_2	$R^{[--]}$	8(b)
$[\xi_k^2, \xi_k^3]$	C_2	$C^{[b]}$	8(c)
$[\xi_k^3, \xi_k^4]$	H_1	$H^{[R]}$	8(d)
$[\xi_k^4, \xi_k^5]$	C_1	$C^{[b]}$	8(e)
$[\xi_k^5, \xi_k^6]$	H_2	$H^{[m]}$	8(f)
$[\xi_k^6, \xi_k^7]$	R_3	$R^{[e]}$	8(g)

Table 2: Wave parts, Example 1.

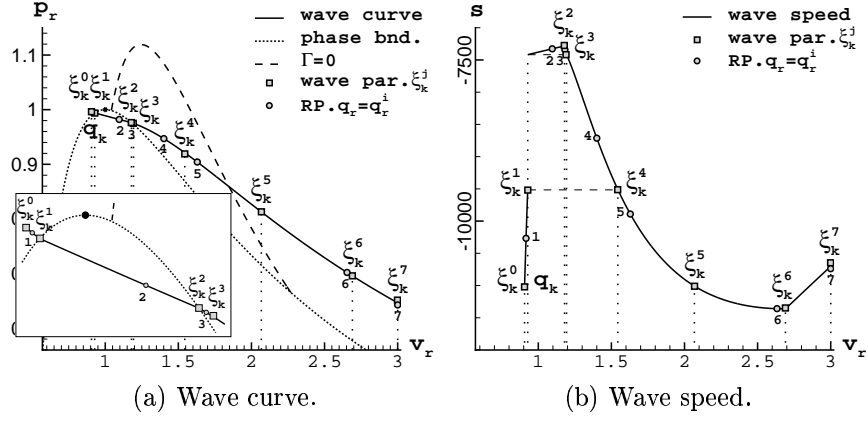


FIGURE 7. Wave characteristics, Example 1.

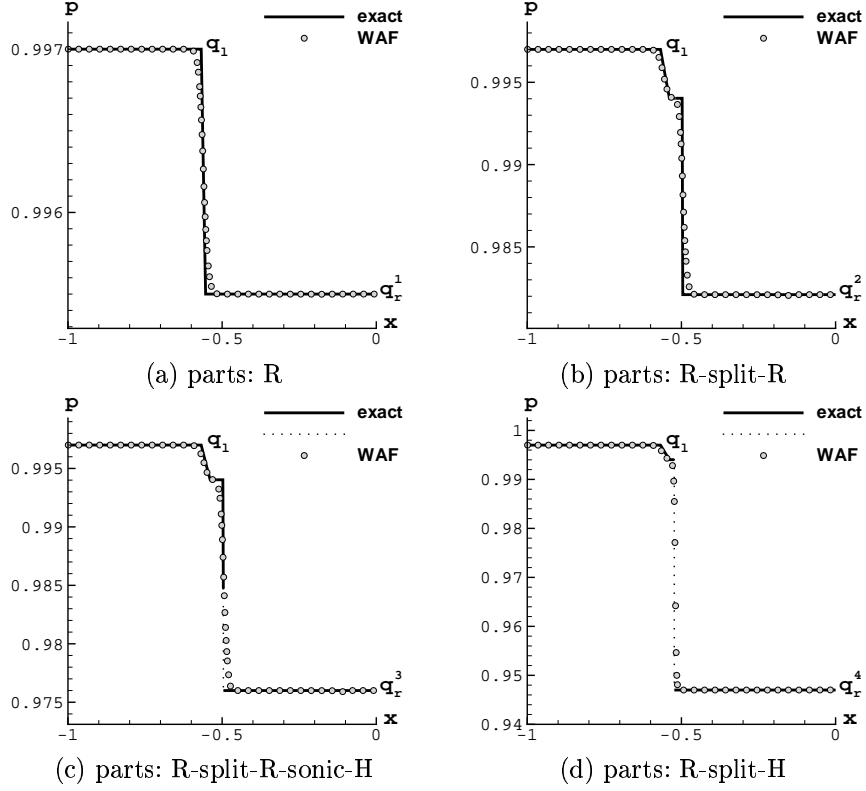


FIGURE 8. to be continued

sequel to FIGURE 8.

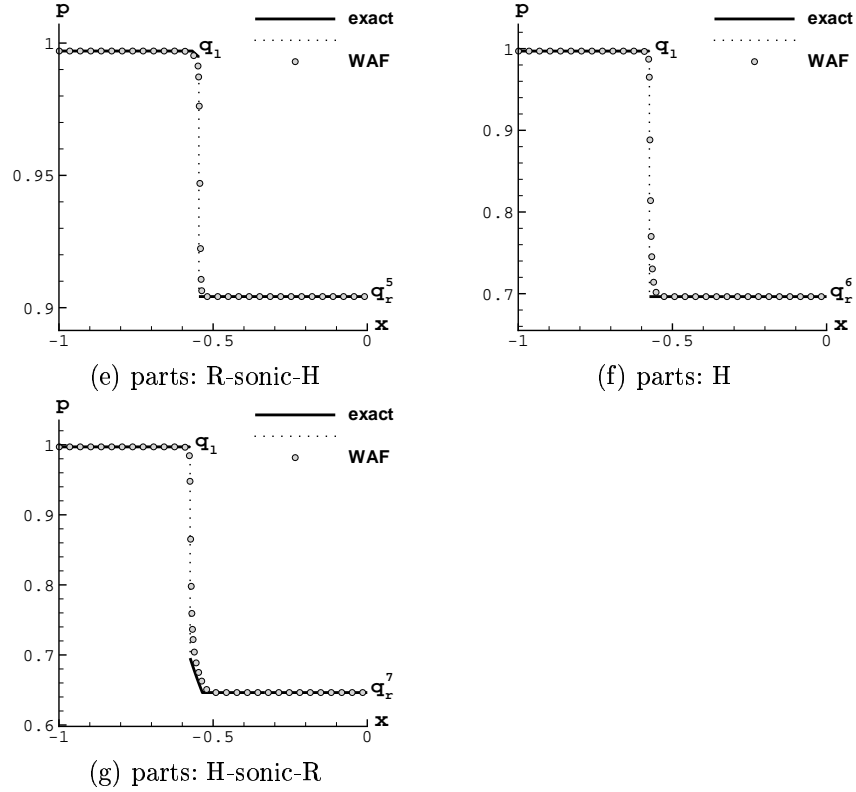


FIGURE 8. Pressure in space for different Riemann problems at constant time.

5 Numerical Results

We consider two types of numerical experiments where phase transition occurs in the flow field. First, we investigate a liquefaction shock expanding from a shock tube into an observation chamber. Another configuration concerns the collapse of a planar bubble near a rigid wall. The two configurations are shown in Figure 9.

The numerical simulations are performed by the solver QUADFLOW, see [BGMH⁺03]. This is a finite volume solver for block-structured grids. In each block we perform grid adaptation by means of a multiscale analysis. The convective fluxes are determined by solving quasi-one dimensional Riemann problems at the cell interfaces. Here we use the Roe Riemann solver adapted to real gas. The spatial accuracy is increased by a linear, multidimensional reconstruction of the conservative variables. In order to avoid oscillations in the vicinity of local extrema and discontinuities, limiters with TVD property

are used. The time integration is performed by an explicit multistage Runge–Kutta scheme.

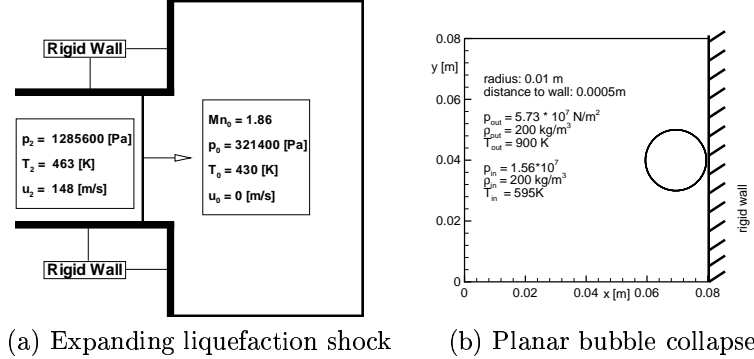


FIGURE 9. Initial configurations.

5.1 Expansion of a Liquefaction Shock

The setting of this configuration is sketched in Figure 9 (a). The fluid under consideration is the high-molecular fluorcarbon FC75. In a shock tube of radius $r = 0.288$ m a “liquefaction shock” is generated. Here the pre-shock state q_0 and the post-shock state q_2 are chosen such that they are lying on the same Hugoniot curve which crosses both phase boundaries connecting the state q_2 in the *liquid phase* by the state q_0 in the *vapor phase*. In Figure 10 the wave curve and the initial states are shown in the p - v -diagram. The liquefaction shock is running to the right and is expanding into the observation chamber. This results in a diffraction of the planar shock wave. It has been investigated experimentally, see [Tho91]. According to Section 3 we apply the van der Waals EOS with Maxwell’s construction principle. The critical values of the fluid FC75 are $v_c = 0.0017$ kg/m³, $T_c = 500.21$ K, $p_c = 0.1607 \times 10^7$ Pa.

Notable features of the axisymmetric, unsteady flow are the strong vortex and the Prandtl-Meyer expansion characteristics. An internal shock originates near the vortex center. This is depicted in Figure 15. The structure of the extreme expansion fan is referred to as the “Mach trumpet”, see [Tho91]. The main compression shock forms the front of the trumpet whereas the sides are formed by a rarefaction shock. The rarefaction shock is of the mixture-evaporation type. It is associated to the kink of the isentropes at the saturated-vapor boundary. To validate this we extract data along a particle path crossing the shock front and project the corresponding states in the p - v diagram, see Figure 11. The streamline is depicted from Figure 15. In addition, we present in Figure 16 the different regions in the flow field where the fluid undergoes a phase transition. At the phase boundaries the sound speed jumps due to

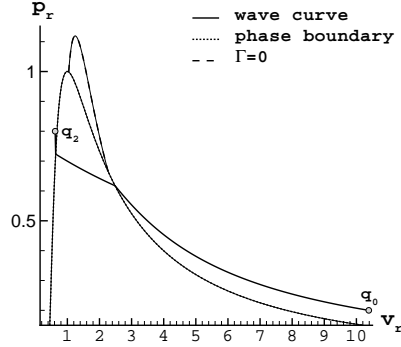


Fig. 10. Wave curve with initial data

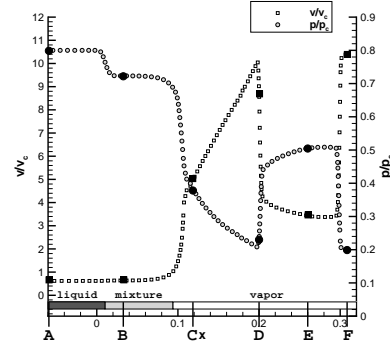


Fig. 11. Data extracted from stream-line

the kink of the isentropes in the p - v diagram. These discontinuities can be depicted from the Mach contours in Figure 14.

5.2 Bubble Collapse near a rigid Wall

We consider a cylindrical bubble filled with water steam surrounded by water near a planar solid wall. The water is at high pressure and high temperature. The fluid inside the bubble is at low pressure (below vapor pressure) and lower temperature corresponding to wet steam, i.e., the state lies inside the mixture region. Both states are at constant volume. This configuration is sketched in Figure 9 (b). Here the fluid water is modeled by the van der Waals EOS applying Maxwell's construction principle modeling the mixture region. The critical values are $v_c = 0.0018016 \text{ kg/m}^3$, $T_c = 647.4 \text{ K}$, $p_c = 0.2212 \times 10^8 \text{ Pa}$. The initial conditions correspond to a Riemann problem where three types of waves occur: an inward running compression shock, an outward running rarefaction wave and a contact discontinuity. The outward running rarefaction is visible in the pressure as well as the density whereas the contact discontinuity is only seen in the density. At time $t = 3.01 \mu\text{s}$ the rarefaction wave is reflected at the rigid wall. Due to a superposition of the rarefaction wave and the reflected rarefaction wave a low pressure region develops between the bubble and the wall. The reflected rarefaction wave is running over the contact discontinuity and the shock wave. Due to the pressure drop behind the reflected rarefaction wave the fluid is accelerated towards the wall and, hence, the bubble starts moving towards the wall and the bubble surface is deformed, see Figure 17 (c)–(h). Since the acoustic impedance is about three times higher in the water phase than in the wet steam phase the rarefaction wave is running faster than the shock wave. At time $t = 13.93 \mu\text{s}$ the inward running shock has reached the center of the bubble and is reflected, see Figure 17 (g), (h). Behind the shock the pressure increases above vapor pressure and the wet steam vaporizes. The reflected shock wave is running

over the contact discontinuity, see Figure 17 (i), (j), and the fluid behind the shock is accelerated in outward direction. Therefore mass is transported away from the bubble center and a low pressure region develops near the bubble center, see Figure 17 (k), (l). At time $t = 28.30 \mu\text{s}$ parts of the reflected shock are reflected at the wall. Due to the curved shock front the angle condition is violated and, hence, a Mach stem is developing. The Mach stem becomes stronger with increasing time propagating away from the symmetry line, see Figure 17 (k)–(r). Again the reflected shock wave is running over the bubble and the mass behind the wave accelerated in the direction of the moving shock front. Therefore the fluid is accelerated away from the wall which leads to an additional deformation of the bubble shape compensating for the previous deformation. Finally, the bubble shape becomes almost symmetric again. In particular, the bubble does not interact with the wall and we do not observe a collapse of the bubble.

Acknowledgement. The authors would like to thank Prof. Dr. Josef Ballmann and Dipl.-Phys. Sigrid Andreae, Lehr- und Forschungsgebiet für Mechanik, RWTH Aachen, for the fruitful cooperation within the DFG-Priority Research Program *Analysis and Numerics for Conservation Laws*. In particular, the discussions on the physical modeling have been very helpful.

References

- [BBKN83] A.A. Borisov, Al.A. Borisov, S.S. Kutateladze, and V.E. Nakoryakov. Rarefaction shock wave near the critical liquid vapor point. *J. Fluid Mech.*, 126:59–73, 1983.
- [BGMH⁺03] F. Bramkamp, B. Gottschlich-Müller, M. Hesse, Ph. Lamby, S. Müller, J. Ballmann, K.-H. Brakhage, and W. Dahmen. H-Adaptive Multiscale Schemes for the Compressible Navier-Stokes Equations — Polyhedral Discretization, Data Compression and Mesh Generation. In J. Ballmann, editor, *Numerical Notes on Fluid Mechanics*, volume 84, pages 125 – 204. Springer, 2003.
- [DTMS79] G. Dettleff, P.A. Thompson, G.E.A. Meier, and H.-D. Speckmann. An experimental study of liquefaction shock waves. *J. Fluid Mech.*, 95(2):279–304, 1979.
- [FH84] G.R. Fowles and A.F.P. Houwing. Instability of shock and detonation waves. *Phys. Fluids*, 27:1982–1990, 1984.
- [Kon57] V.M. Kontorovich. Concerning the stability of shock waves. *Sov. Phys: Tech. Phys.*, 6:1179–1181, 1957.
- [Lam72] K.C. Lambrakis. *Negative- Γ fluids*. PhD thesis, Rensselaer Polytechnic Institute, 1972.
- [Liu74] T.-P. Liu. The Riemann problem for general systems 2×2 conservation laws. *Am. Math. Soc.*, 199:89–112, 1974.
- [Liu75] T.-P. Liu. The Riemann problem for general systems of conservation laws. *J. Diff. Eqns.*, 18:218–234, 1975.

- [Liu76] T.-P. Liu. The entropy condition and the admissibility of shocks. *J. Math. Anal. Appl.*, 53:78–88, 1976.
- [MP89] R. Menikoff and B.J. Plohr. The Riemann problem for fluid flow of real materials. *Rev. Mod. Physics*, 61:75–130, 1989.
- [MV01] S. Müller and A. Voss. On the existence of the composite curve near a degeneration point. Preprint IGPM, RWTH Aachen, 2001.
- [Smi79] R.G. Smith. The Riemann problem in gas dynamics. *Trans. Amer. Math. Soc.*, 249(1):1–50, 1979.
- [TCK86] P. Thompson, G. Carafano, and Y.-G. Kim. Shock waves and phase changes in a large-heat-capacity fluid emerging from a tube. *J. Fluid Mech.*, 166:57–92, 1986.
- [TCM⁺87] P.A. Thompson, H. Chaves, G.E.A. Meier, Y.-G. Kim, and H.-D. Speckmann. Wave splitting in a fluid of large heat capacity. *J. Fluid Mech.*, 185:385–414, 1987.
- [Tho72] P. Thompson. *Compressible Fluid Dynamics*. Rosewood Press, Troy, New York, 1972.
- [Tho91] P. Thompson. Liquid–vapor adiabatic phase changes and related phenomena. In A. Kluwick, editor, *Nonlinear waves in real fluids*, pages 147–213. Springer, New York, 1991.
- [TK83] P. Thompson and Y.-G. Kim. Direct observation of shock splitting in a vapor-liquid system. *Phys. Fluids*, 26(11):3211–3215, 1983.
- [Voßa] A. Voß. *Flows in Fluids with Non-Convex Equation of State*. PhD thesis. In preparation.
- [Voßb] A. Voß. A Numerical Library for Fluids and Convex and Nonconvex EOS including Phase Transition. In preparation.
- [Wen72a] B. Wendroff. The Riemann problem for materials with nonconvex equations of state, I: Isentropic flow. *J. Math. Anal. Appl.*, 38:454–466, 1972.
- [Wen72b] B. Wendroff. The Riemann problem for materials with nonconvex equations of state, II: General flow. *J. Math. Anal. Appl.*, 38:640–658, 1972.

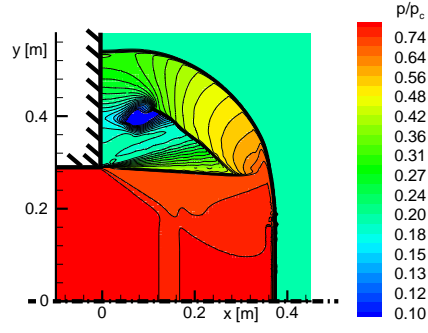


Fig. 12. Pressure contours

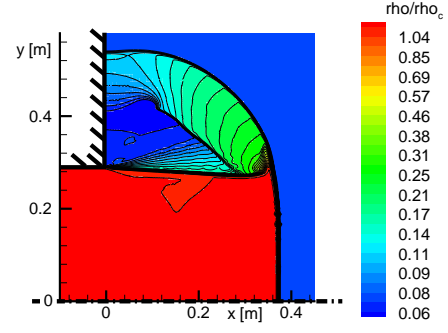


Fig. 13. Density contours

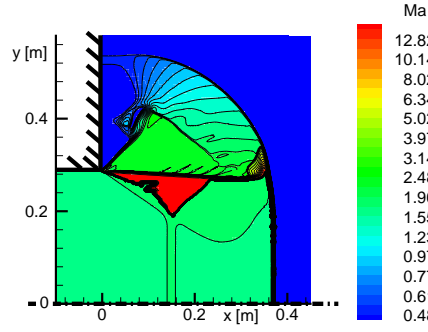


Fig. 14. Mach contours

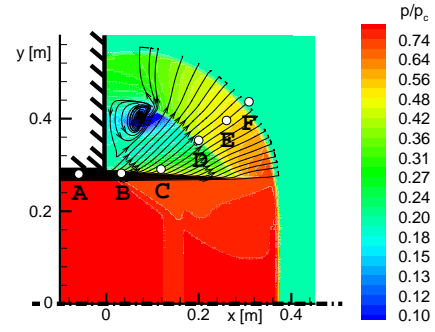


Fig. 15. Streamlines and pressure field

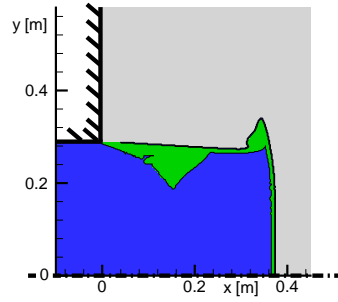


Fig. 16. Fluid phases: liquid (blue), wet steam (green), vapor (grey)

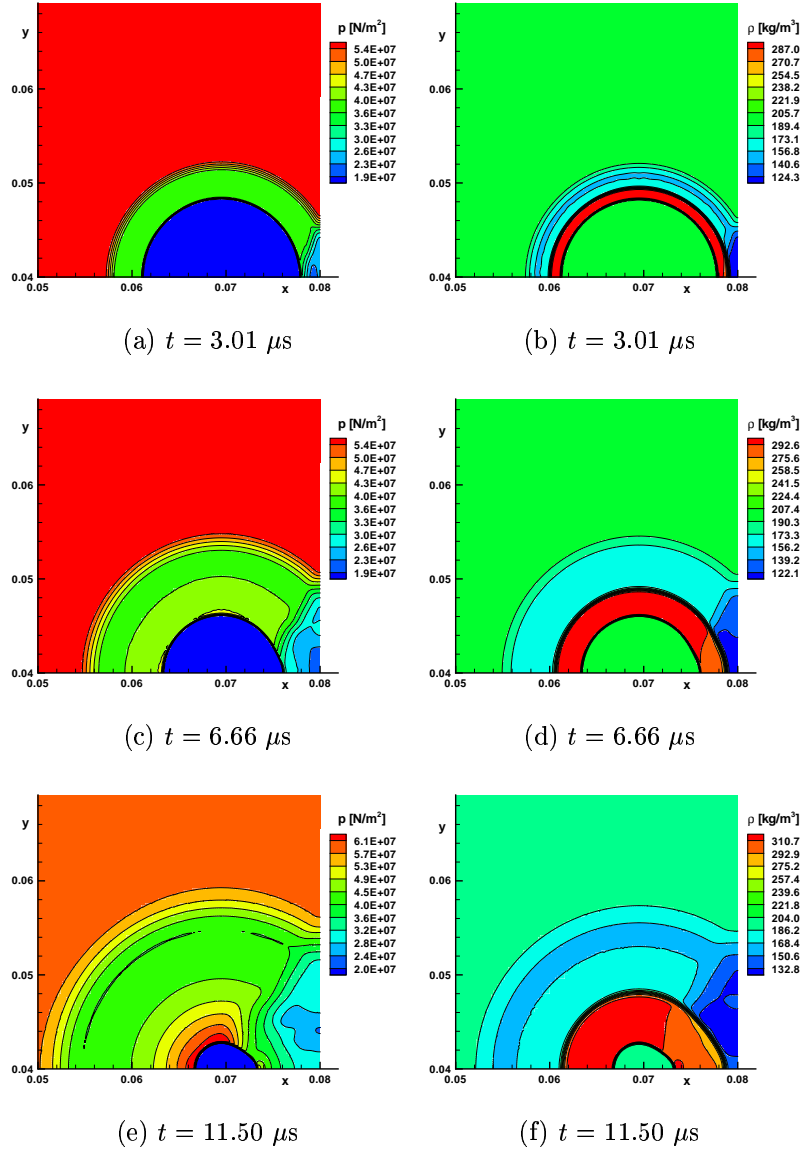


FIGURE 17. to be continued

sequel to FIGURE 17.

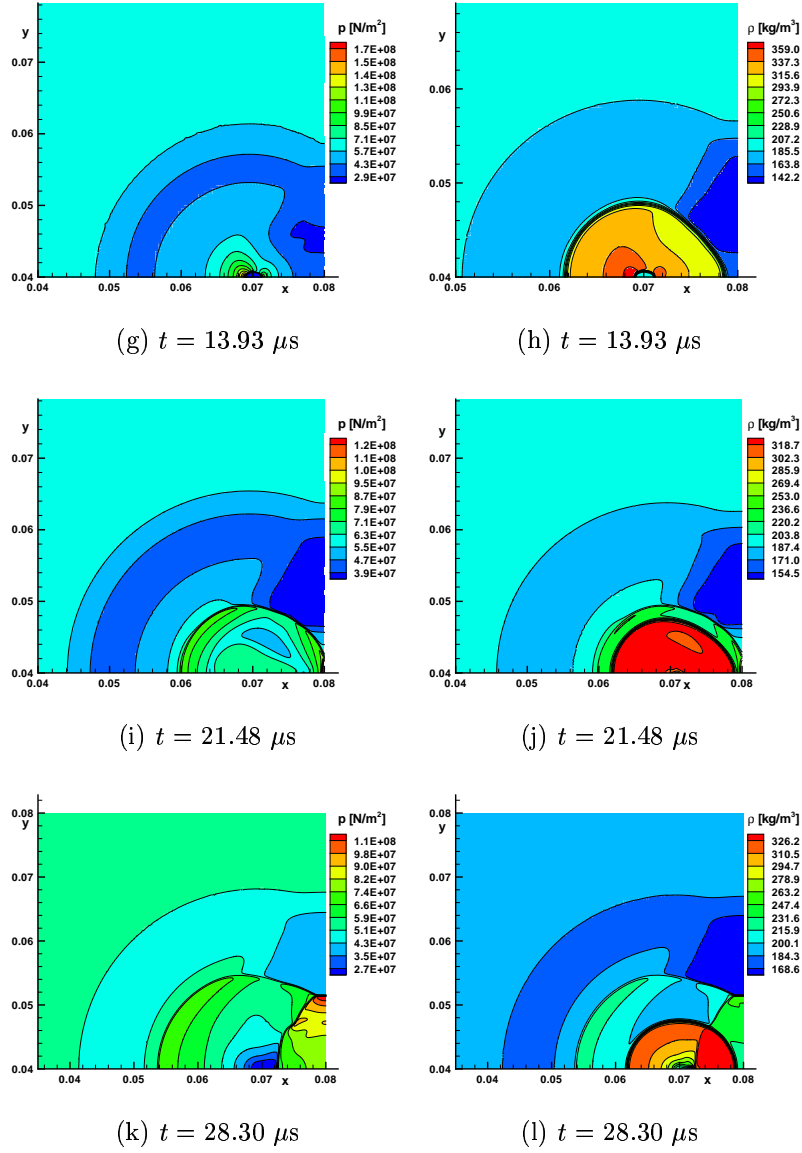


FIGURE 17. to be continued

sequel to FIGURE 17.

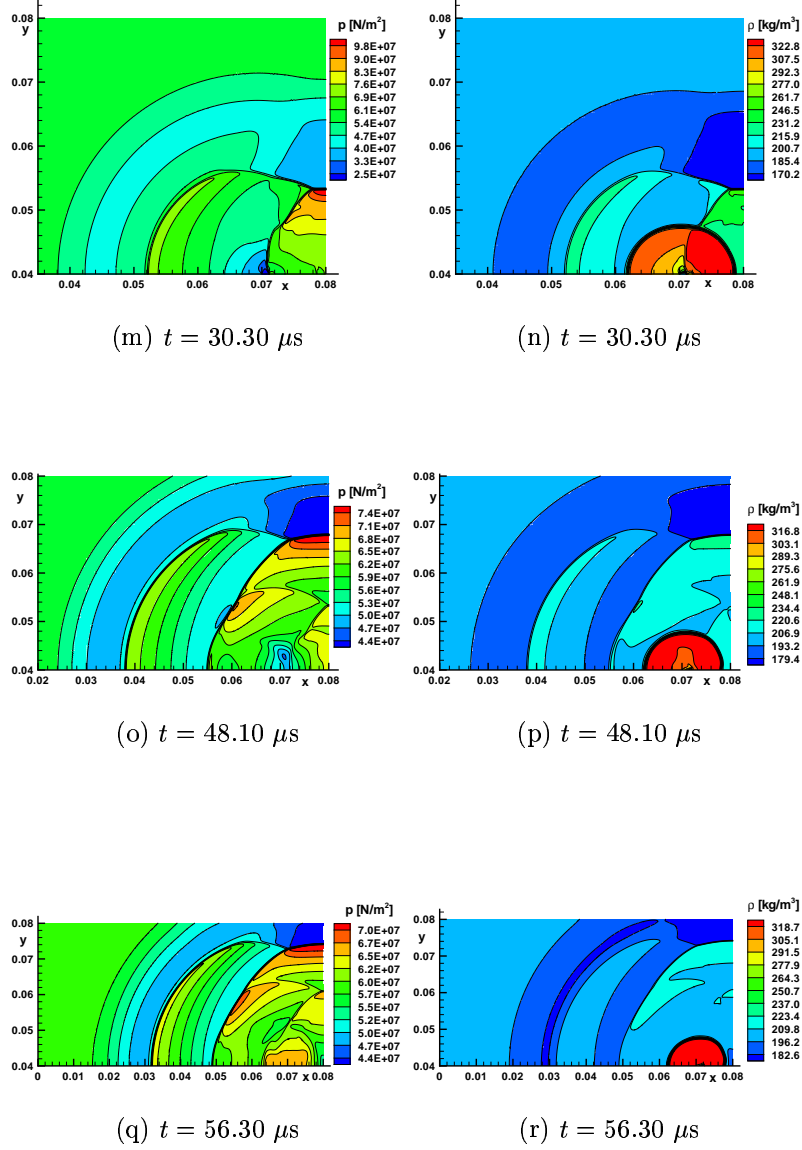


FIGURE 17. Bubble collapse.